

Improved composite spectra of quasars within the H I Ly α -forest region

Ivashchenko G.^{1*}, Sergijenko O.^{2†}, Torbaniuk O.^{3‡}

¹*Astronomical Observatory of the Taras Shevchenko National University of Kyiv, Observatorna str., 3, 04058, Kyiv, Ukraine*

²*Astronomical Observatory of the Ivan Franko National University of Lviv, Kyryla i Methodia str., 8, 79005, Lviv, Ukraine*

³*Faculty of Physics of the Taras Shevchenko National University of Kyiv, Glushkova ave., 4, 03127, Kyiv, Ukraine*

Accepted _____ Received _____; in original form _____

ABSTRACT

We present a new more accurate approach to the composite spectra construction based on stacking spectra with similar slopes α_λ within the wavelength range redward of Ly α emission line, which allows to reduce a noise. With the help of this technique a detailed study of the H I Ly α -forest region ($\lambda_{\text{rest}} \approx 1050 - 1200 \text{ \AA}$) of the own sample of 3,439 medium-resolution quasar spectra from SDSS DR7 was performed. More than 14 lines were found within it, three of which were found in previous studies of quasar composite spectra from SDSS and some others were found in composite spectra from space-based telescopes or high-resolution spectra of individual quasars from ground-based telescopes. The parameters of these lines were calculated. It was shown that the continuum level within the Ly α -forest region cannot be considered as a power-law with the same slope as in the region redward of Ly α emission line. Any dependence of the slope α_λ on luminosity in SDSS u , g , r and i bands as far as on luminosity in 1450 – 1470 \AA band was not found. The proposed approach can be applied for generation of new templates for more precise quasar redshift measurements, theoretical determination of K-correction and color-indexes, as far as for determination of continuum and mean transmission in Ly α forest studies. It was shown that the uncertainties in the mean transmission caused by using the composite spectra made with common approach can constitute about 20%.

Key words: quasars: emission lines — quasars: general

1 INTRODUCTION

The Ly α forest in the spectra of distant quasars traces the thermal and radiative history of the Universe, as well as the evolution of underlying matter distribution over a wide range of scales and redshifts. It is possible due to relation of the Ly α opacity of the intergalactic neutral hydrogen H I to its density and other physical parameters. As a measure of opacity the value F named the transmission is used; fluctuations of it, δ_F , provide an invaluable information about the density fluctuations on the smallest scales available today for observations (Kim et al. 2004; McDonald et al. 2006; D’Odorico et al. 2006; Cappetta et al. 2010).

Two important steps in these studies, after the row spectral data reduction and before calculation of the two-point statistics (correlation function and power spec-

trum) of transmission fluctuations are (i) determination of the redshift-dependent mean transmission \bar{F} level (around which one measures the fluctuations) and (ii) determination of the intrinsic quasar spectrum (transmission of which one measures). For today several tens of high-resolution ($R \sim 100,000$) quasar spectra and several thousands of medium-resolution ($R \sim 2,000$) ones are available for Ly α -forest study. The first ones are obtained with spectrographs like UVES on VLT (see e.g. Kim et al. (2004)) and allow a good spatial resolution for two-point statistics, but using them along one cannot be sure about the reliability of the mean transmission level for a given redshift due to small number of spectra. Moreover in this case the quasar continuum is fitted manually with the spline polynomials without any underlying ideas about the emission lines’ shape etc., that can result in additional uncertainties. It is worth to note, that the term *continuum* in this case usually means the whole intrinsic quasar spectrum including emission lines. We follow this definition and refer to the continuum without emission lines as the *true continuum*. The medium-resolution

* E-mail: g.ivashchenko@gmail.com

† E-mail: olka@astro.franko.lviv.ua

‡ E-mail: el.torbaniuk@gmail.com

spectra are obtained mainly in the scope of the Sloan Digital Sky Survey (SDSS) project (Abazajian et al. 2009). They can serve well for the mean transmission determination, but they do not allow the manual direct fitting of the continuum within the Ly α -forest part because it is almost impossible to find unabsorbed regions in such spectra.

For calculations of the mean transmission and continuum level in the case of medium resolution spectra the so-called composite (mean) spectra are used. The possibility of their utilization is related to the fact that quasar spectra are remarkably similar from one object to another. Such ultraviolet-optical spectra can be characterized by a featureless continuum and a series of mostly broad emission line features; and due to their high signal-to-noise ratio these spectra also reveal weak emission features that are rarely detectable in individual quasar spectra. The composite spectra were compiled for a wide set of quasar samples, e.g. the Large Bright Quasar Survey (LBQS) (Francis et al. 1991), the First Bright Quasar Survey (FBQS) (Brotherton et al. 2001), the SDSS (Vanden Berk et al. 2001; Pieri et al. 2010), quasar spectra from the Hubble Space Telescope (HST) (Zheng et al. 1997; Telfer et al. 2002) and Far Ultraviolet Spectroscopic Explorer (FUSE) (Scott et al. 2004).

The part of UV-optical quasar spectrum redward of the Ly α (1215.67 Å) emission line (free of hydrogen Lyman-series forests of absorption lines) is studied quite well. As it was shown e.g. by Vanden Berk et al. (2001) this region up to ≈ 5000 Å is described well with a smooth power-law shape $\sim \lambda^{\alpha_\lambda}$ of the true continuum and broad emission lines. Vanden Berk et al. (2001) reported on α_λ to be -1.54 within 1350–4230 Å, that agrees well with the values -1.54 and -1.68 which were obtained by Brotherton et al. (2001) within 1450–5050 Å for spectra from LBQS and FBQS correspondingly, and also with the results of Carballo et al. (1999), who obtained the values -1.34 ± 0.15 and -2.11 ± 0.16 within 1300–3000 Å and 3000–4500 Å ranges correspondingly for a sample of radio-loud quasars. Throughout this paper the wavelengths mean rest-frame ones, unless otherwise is specified.

The part of the spectrum blueward of Ly α emission line, or strictly speaking the part of spectrum between doublet of Ly β (1025.72 Å) – O VI (1033.83 Å) and Ly α , which is used for the Ly α forest region studies, is much less better investigated due to the presence of the Ly α forest itself. There are two techniques used for continuum level determination within this region. The first one lies in the direct fitting, usually by polynomials, of it within the Ly α forest region in high-resolution spectra (McDonald et al. 2000; D’Odorico et al. 2006; Becker et al. 2007; Faucher-Giguère et al. 2008). For medium-resolution spectra, where it is difficult to select unabsorbed regions, another technique is applied: it is based on extrapolation of the true continuum level from the red side of the Ly α emission line, that is free from H I absorption with addition of several emission lines or without it and determination of continuum level directly in the Ly α region modeling the spectrum with the several-parametric model including the mean transmission and parameters of emission lines (Press et al. 1993; Bernardi et al. 2003; Desjacques et al. 2007; Polinovsky & Malygin 2010; Songaila 2004). More complicated, but similar to the last one, method was proposed by McDonald et al. (2006). Instead of using composite

spectra these authors worked with a whole sample of individual spectra and applying the principal component analysis found the mean continuum level, mean transmission and mean generalized calibration vector, a function defined by them to include calibration errors and mean absorption by metal lines with $\lambda > 1300$ Å, and also their fluctuations.

Several-parametric modelling of the continuum level within the Ly α forest region suffers from the degeneration between the mean transmission and parameters of the true continuum, that is why extrapolation of the true continuum from the red part of spectrum seems to be much reliable. But in practice it is only an approximation of the true continuum because of the fact that the peak of the well-known big blue bump in quasar spectra is located within 1000–1300 Å region. This is confirmed by the values of α_λ obtained from HST and FUSE spectra, -1.01 ± 0.05 within 1050–2020 Å (Zheng et al. 1997), -0.24 ± 0.12 within 500–1200 Å (Telfer et al. 2002), $-1.44^{+0.38}_{-0.28}$ within 630–1155 Å (Scott et al. 2004), when comparing with the same values for longer wavelengths mentioned above. Hence the several-parametric modelling is left to be the most reliable method. But except the degeneration of parameters its usage encounters another problem, the choice of the model for the continuum level. Usually a superposition of the power-law and three Gaussians is considered. These Gaussians present three broad emission features, two around 1073 Å and 1123 Å and Ly α line. The values of 1073 Å and 1123 Å were found by Bernardi et al. (2003) and used by Desjacques et al. (2007). But there are also other estimations of these values. E.g. Vanden Berk et al. (2001) measured them to be 1065.10 Å and 1117.26 Å from the SDSS quasar composite spectrum and referred to them as Ar I ($\lambda_{lab} = 1066.66$ Å) and Fe III multiplet; they also found one more emission line, C III* ($\lambda_{lab} = 1175.67$ Å) with the wavelength 1175.35 Å, within Ly α -forest region. The same emission features were found by Tytler et al. (2004) to be 1070.95 Å, 1123.13 Å and 1175.88 Å correspondingly. More close look to these emission features during the traditional modelling mentioned above and performed by us showed that the values of these central wavelengths vary significantly from spectrum to spectrum and the ‘line’ profiles in some cases are far enough from symmetric Gaussians. These conclusions together with the results on the space-based composite UV spectra of the nearest quasars (Telfer et al. 2002; Scott et al. 2004) and ground-based individual optical spectra of some quasars (Binette & Krongold 2008; Leighly et al. 2007) led us to the idea of the improvement of the model. One of the main sources of uncertainties during the generation of the composite spectrum lies in a fact that despite of their similarities in general the quasar spectra differ in the slopes of the true continuum level in the red part of UV-optical bump. Thus we tried to generate the composite spectra from the samples of spectra with the similar α_λ .

The data used in this work, the sample selection and the composite spectra generation processes are described in Section 2. The methods of lines identification and calculation of their parameters are presented in Section 3. The results and their discussion are presented in Section 4. Finally Section 5 contains the discussion of obtained results.

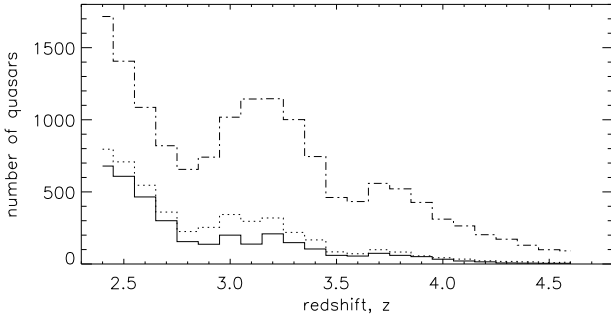


Figure 1. Redshift distribution of all objects from the HW sample with $2.3 < z < 4.6$ and redshift determination confidence level > 0.9 (*dash-dot*), all visually selected (*dotted*) for the present study and those with the rms of the normalization constant A less than 15% (*solid*).

2 DATA

2.1 The SDSS DR7 quasar sample

Our sample is taken from the public available release of the sky-residual subtracted spectra for the Sloan Digital Sky Survey (SDSS) Legacy Release 7 (Abazajian et al. 2009). This release (‘WH sample’ hereafter), which is described in Wild & Hewett (2010), contains a total of 106,006 spectra, generated using the Wild & Hewett (2005) scheme from the spectra of the objects from the Schneider et al. (2010) quasar catalogue. This scheme includes a significantly improved technique of the OH sky lines subtraction. The strong OH sky emission lines extend over almost half of the wavelength range ($> 6700 \text{ \AA}$) of the SDSS spectra and is not subtracted optimally enough with the previous SDSS pipelines.

The redshifts in SDSS are measured mainly with the help of two techniques — emission line measurements and cross-correlation, or one of them. The errors of redshift (due to intrinsic line shifts etc.) could affect the results of our study hence we tried to minimize their influence using the improved redshifts of the objects from the Schneider et al. (2010) quasar catalogue, which was generated using the Hewett & Wild (2010) scheme, instead of redshifts in the headers of each fits-file. According to Hewett & Wild (2010), their redshifts possess systematic biases, which are a factor of 20 lower compared to the SDSS redshift values.

2.2 Spectra selection

All the quasar spectra (15,154 objects) from the HW sample with redshifts within the range $2.3\text{--}4.6$ and redshift determination confidence level > 0.9 were firstly selected. Because the SDSS is an automatic survey there is a possibility of pollution of the sample with ‘wrong’ objects whose general photometry or spectroscopy properties required by the automatic selection pipelines are similar to the ones of ‘real’ objects. Thus a visual examination was carried out. Except the non-quasar spectra the spectra of quasars with low signal-to-noise ratio, broad absorption lines (BAL) and Damped Ly α (DLA) systems were also excluded during this examination.

The usual formal definition of BAL quasar is a quasar with a positive balnicity index (a measure of the equivalent

width of the C IV absorption) (Weymann et al. 2001). Their spectra show broad ($\sim 2000\text{--}20000 \text{ km/s}$, sometimes up to $66,000 \text{ km/s}$), blueshifted absorption troughs corresponding to highly-ionized rest-frame-UV resonance transitions such as C IV, Si IV, N V, O VI, more rarely Mg II and Al III, and even more rarely Fe II (see e. g. Menou et al. (2001)). The similarity of the continuum and line emission of BAL and non-BAL quasars motivates the hypothesis that BAL quasars are not intrinsically different from other quasars and the presence of BAL features in the spectra of only $\sim 10\%$ of optically selected quasars is usually explained by a difference in viewing angle if the subrelativistic outflow at the origin of BAL features is non isotropic. The popular notion is that the outflow is preferentially located in the plane of the disc surrounding the supermassive black hole. The presence of the BAL quasars in the sample could introduce additional errors into an estimation of the quasar mean continuum level.

The DLA systems are a class of quasar absorbers selected for the presence of H I column densities $> 2 \cdot 10^{20} \text{ cm}^{-2}$ (see e. g. Wolfe et al. (2005) for review). They are identified as absorption features with the rest equivalent width exceeding 5 \AA . The nature of these systems is still not understood, however due to their high density they are usually related to the galaxy formation and therefore could not be used as representatives of the linear perturbations in the neutral intergalactic medium.

After the visual examination the sample contains 4,779 spectra. Redshift distributions of these objects and all the objects initially selected from HW sample are presented in Figure 1 (*dash-dot* and *dotted* correspondingly).

2.3 Generating composite spectra

Generating composite spectra of quasars includes three steps: (i) normalization of each spectrum, (ii) setting each spectrum to the rest frame and (iii) calculation of the mean spectrum. Before we smoothed all spectra with a simple moving average over 3 points. Following McDonald et al. (2006) we removed the following wavelength regions from our analysis because of calibration problems due to strong sky lines: $5575 \text{ \AA} < \lambda < 5583 \text{ \AA}$, $5888 \text{ \AA} < \lambda < 5895 \text{ \AA}$, $6296 \text{ \AA} < \lambda < 6308 \text{ \AA}$, and $6862 \text{ \AA} < \lambda < 6871 \text{ \AA}$, where the second region is 1 \AA wider than that presented in McDonald et al. (2006), because we added also Na I (5894.6 \AA) interstellar line to it. Normalization of each spectrum is needed to be applied due to different apparent flux densities. Taking into account the similarity of quasar spectra and following Press et al. (1993) and Zheng et al. (1997) we normalize each spectrum on the (arithmetic) mean flux in all pixels within the rest wavelength range $1450\text{--}1470 \text{ \AA}$. This range lies blueward from the C IV emission line and is usually considered to be free of obvious emission and absorption. The last claim appears to be not precise because of the weak emission line, which can be seen in composite spectra, but we neglect this fact, because intensity of this line is compared with noise level in individual spectra. For further study to reduce possible uncertainties we used only spectra with the rms of the normalization constant A less than 15%; the number of them is 3,493 and its redshift distribution is shown in Figure 1 (*solid* line).

Considering the true continuum of the quasar spectra redward of Ly α emission line to be a power-law $\sim \lambda^{\alpha_\lambda}$,

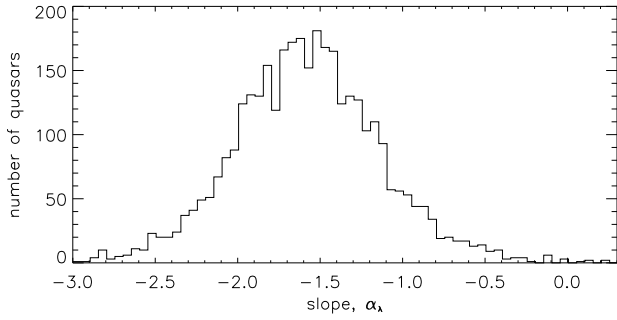


Figure 2. The distribution of the true continuum slopes redward of $\text{Ly}\alpha$ emission line.

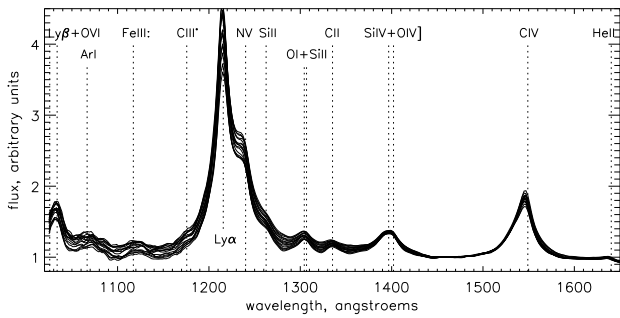


Figure 3. Composite spectra of 16 subsamples within 1025–1650 Å. The highest spectrum has the steeper true continuum redward of $\text{Ly}\alpha$ emission line.

we calculated its slope α_λ for each individual spectrum within the range between $\text{Ly}\alpha$ and $\text{CIV}(1549.0\text{ Å})$ emission lines. For this purpose we selected the following wavelength ranges from the composite spectrum compiled from all the spectra: 1278–1286 Å, 1320–1326 Å, 1345–1360 Å and 1340–1480 Å. The distribution of the obtained slopes is shown in Figure 2.

Using the obtained values of α_λ , we selected 16 subsamples each of 200 spectra with α_λ closest to $-0.7 - k \cdot 0.1$, $k = 0.15$. Then dividing each j -th selected spectrum onto its normalization constant A^j , rebinning them with $\Delta\lambda_{\text{rest}} = 2\text{ Å}$ and stacking the spectra into the rest frame, we obtained the mean arithmetic composite spectra. The dispersion σ^2 of each pixel of the composite spectrum was calculated from the noises σ_i of pixels of individual spectra constituting it as $\sigma^{-2} = \sum_i \sigma_i^{-2}$. These spectra within 1025–1650 Å and enlarged part within 1025–1200 Å are shown in Figures 3 and 4 correspondingly. The dashed lines indicate the laboratory wavelengths of the indicated lines identified by Vanden Berk et al. (2001) in this range. The slopes of these composite spectra, calculated as mentioned above, with the errors of approximation, and also the mean redshift and the mean absolute magnitude in SDSS i -band \bar{M}_i of each subsample with their rms are presented in Table 1.

The slopes of the true continuum in this case were calculated in the way mentioned above, but the parts of the spectra which are the most free from emission lines were selected manually in each spectrum. The part of spectra used for calculation of the true continuum slope is shown in Figure 5 (*short-dashed* line, the highest spectra are the steepest ones). The three spectra with the slopes -0.84 , -1.49 and

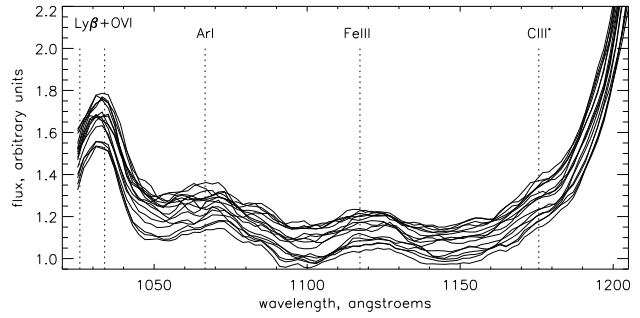


Figure 4. The same as in Fig. 3 within 1025–1200 Å.

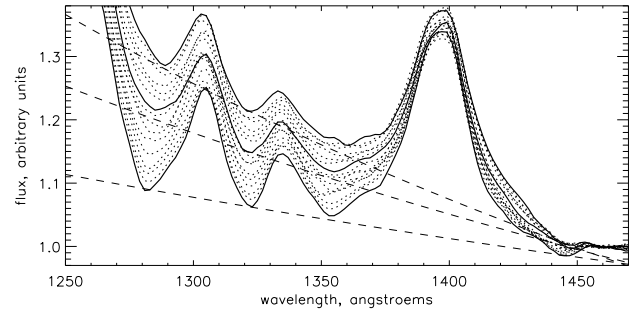


Figure 5. The parts of the composite spectra used for true continuum approximation. See explanation in the text.

-2.12 are shown with the *solid* lines together with the fitted power-law true continua (*dashed* lines). The regions which were used for fitting the true continuum slightly vary from spectrum to spectrum and not all four parts used in calculation of the slopes of the individual spectra we taken into account in the case of composite spectra. This is obviously seen on an example of the region with the shortest wavelengths: with the steepening of the spectrum the centre of it moves from $\sim 1280\text{ Å}$ to $\sim 1290\text{ Å}$. It means that approximation of the true continuum using the same regions as it was done for individual spectra is only an approximation, but this approximation is sufficient for rough separation of spectra for composites compilation.

The values of absolute magnitudes in i -band, M_i , for each individual object were taken from the Sloan Digital Sky Survey Quasar Catalog V (Schneider et al. 2010), where it is calculated within the frame of the flat Λ CDM cosmological model with $H_0 = 70\text{ km/s/Mpc}$, $\Omega_M = 0.3$, $\Omega_\Lambda = 0.7$, and correcting for Galactic extinction (using the maps of Schlegel et al. (1998)) and assuming that the quasar spectral energy distribution in the UV-optical can be represented by a power law with $\alpha_\lambda = -1.5$. As one can see, the objects in all subsamples have similar mean redshift and mean absolute magnitude. It means that any possible differences in the spectral properties within the wavelength region under consideration, which can be obtained in course of the present study, cannot be explained by the evolution effects or related to quasar luminosity, at least in i -band.

It is worth to note that the absolute magnitude in i -band usually used as a value characterizing the luminosity of objects is not a good characteristic in case of quasar UV-bump because its mean wavelength is 7481 Å , which is far from the peak of the big blue bump, that is why we

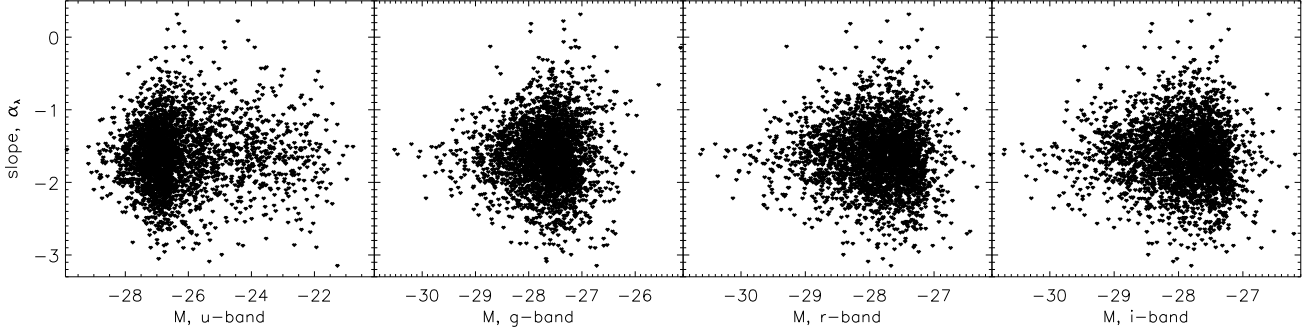


Figure 6. Slope α_λ — absolute magnitude M diagrams for u, g, r, i -bands.

Table 1. Characteristics of 16 subsamples, the mean redshift \bar{z} and the mean absolute magnitude in SDSS i -band, and the slopes α_λ of the their composites.

| n | α_λ | \bar{z} | \bar{M}_i |
|----|------------------|-----------------|-------------------|
| 1 | -0.84 ± 0.04 | 2.90 ± 0.54 | -27.37 ± 0.59 |
| 2 | -0.92 ± 0.03 | 2.89 ± 0.53 | -27.37 ± 0.59 |
| 3 | -0.99 ± 0.02 | 2.87 ± 0.51 | -27.36 ± 0.60 |
| 4 | -1.02 ± 0.05 | 2.85 ± 0.49 | -27.35 ± 0.63 |
| 5 | -1.19 ± 0.02 | 2.82 ± 0.43 | -27.36 ± 0.62 |
| 6 | -1.30 ± 0.02 | 2.84 ± 0.49 | -27.38 ± 0.57 |
| 7 | -1.42 ± 0.03 | 2.82 ± 0.44 | -27.41 ± 0.63 |
| 8 | -1.42 ± 0.02 | 2.76 ± 0.40 | -27.43 ± 0.57 |
| 9 | -1.49 ± 0.05 | 2.77 ± 0.44 | -27.41 ± 0.64 |
| 10 | -1.55 ± 0.03 | 2.80 ± 0.46 | -27.43 ± 0.72 |
| 11 | -1.67 ± 0.01 | 2.75 ± 0.45 | -27.39 ± 0.67 |
| 12 | -1.83 ± 0.04 | 2.75 ± 0.43 | -27.42 ± 0.61 |
| 13 | -1.86 ± 0.04 | 2.74 ± 0.43 | -27.36 ± 0.63 |
| 14 | -1.99 ± 0.03 | 2.72 ± 0.42 | -27.30 ± 0.61 |
| 15 | -2.00 ± 0.02 | 2.74 ± 0.42 | -27.31 ± 0.62 |
| 16 | -2.12 ± 0.03 | 2.74 ± 0.43 | -27.34 ± 0.65 |

plotted also diagrams slope α_λ – absolute magnitude M in u (3551 Å), g (4686 Å), r (6165 Å) along with i -band (Figure 6). These magnitudes we calculated using the apparent psf magnitudes and reddening in corresponding bands from SDSS DR7, K-correction values from Richards et al. (2006) and within the cosmological model mentioned above. As one can see from these diagrams there is no dependence between the slope and absolute magnitudes in these bands, however even the u -band is about 2000 Å far from the bump. Hence we used also the values of A^j as a characteristic of luminosity in this band and plot α_λ – B diagram (Figure 7), where we determined B as a mean flux within 1450 – 1470 Å in case when the object is located 10 Mpc far from an observer, some ‘absolute’ flux, similarly to definition of absolute magnitudes. Extending this analogy of absolute magnitudes we plotted B in logarithmic scales, but also did not find any evidence for dependence of the slope α on luminosity in this band. Generally speaking this range is also not the best choice, but as it was noticed above this one is the most free of obvious emission and absorption features, thus it should be the most appropriate to characterize quasar continuum luminosity within the bump.

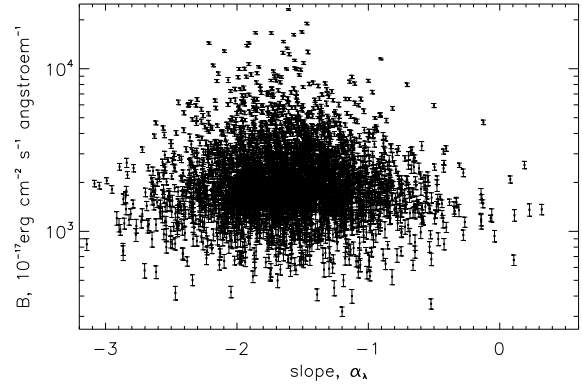


Figure 7. Slope (α_λ) – ‘absolute’ flux within 1450 – 1470 Å (B) diagram.

3 THE TECHNIQUE

3.1 General notations

The data are given in the form of pixels with wavelength label λ_i , the flux density value f_i and noise n_i . Following Bernardi et al. (2003); McDonald et al. (2006) we present the observed flux density f_i^j in i -th pixel within the Ly α forest region of j -th quasar as

$$f_i^j = A^j \bar{C}(\lambda_{rest})(1 + \delta_{C,i}^j) \bar{F}(z)(1 + \delta_{F,i}^j) + n_i^j, \quad (1)$$

where A^j is the normalization constant described above (Sec. 2.3), the wavelength λ_i of the absorption Ly α feature produced by the ‘cloud’ of intergalactic H I is related to its redshift z_i as $\lambda_i = 1215.67(1 + z_i)$, $C(\lambda)$ is the mean continuum level, δ_C are deviations of individual continuum from the mean one, n is the noise, \bar{F} is the mean transmission for a given redshift and δ_F are variance (or fluctuations) of transmitted flux.

Through the fact that different terms of expression (1) depend on different variables, some of them can be determined separately. Namely continuum level $C + \delta_C$ is a function of the rest wavelength λ_{rest} ; mean transmission \bar{F} is a function of redshift, δ_F depends on a line of sight (presented by a given quasar); n_i depends on the instrument properties and conditions of observation thus can be considered as a function of the observed wavelength λ_{obs} ; and A^j is a constant determined in advance. Hence, the mean arithmetic composite spectrum for a given subsample with the mean redshift \bar{z} can be presented as:

$$f(\lambda_{rest}) = \bar{C}(\lambda_{rest}) \bar{F}(\bar{z}), \quad (2)$$

because the values $\langle \delta_{F,i}^j \rangle$, $\langle \delta_{C,i}^j \rangle$ and $\langle n_i^j \rangle$ are equal to zero when averaging over a large number of quasar spectra within a given redshift bin (see e.g. Bernardi et al. (2003) for details). Taking into account the similarity of the mean redshifts for all our subsamples we can consider each our composite spectrum within the Ly α -forest region as $f(\lambda_{rest}) = \bar{F}'\bar{C}(\lambda_{rest})$, where we assume \bar{F}' to be the same for each subsample.

3.2 Modelling the spectra

The mean quasar continuum $\bar{C}(\lambda_{rest})$ within the Ly α forest region can be presented as a sum of the true continuum which is usually assumed to have a power-law form (Bernardi et al. 2003; Desjacques et al. 2007) and emission lines which are fitted well with Gaussian profile because of large velocities of the regions where they are formed. But unlike the common treatment we consider the ‘pure’ continuum of this wavelength region as a constant, not a power-law, due to the following facts. Firstly, it is known (see e.g. Desjacques et al. (2007) for discussion) that extrapolation of the power-law ‘pure’ continuum from the redward part of the spectrum yields to underestimated mean transmission \bar{F} in the Ly α -forest comparing with the results from high-resolution spectra for which continuum fitting within Ly α -forest region is made directly. This difference is usually assigned to large systematic errors, but it is also could be explained by the fact that Ly α -forest region is located near the peak of the Big Blue Bump of quasar spectra, and thus consideration of the ‘pure’ continuum within limited wavelength band, e.g. redward of 1216 Å, as a power-law is just an approximation (indeed a tangent to a real curve determining UV continuum of quasars, the physical model of which is still poorly understood). Secondly, the small width of this region together with existence of the emission lines results in large uncertainties in parameters of the power-law. That is why consideration of such narrow region (≈ 150 Å wide) as a linear (or even a constant in our case) function seems to be precise enough. Hence the fitting formula for the product of the mean transmission and continuum is the following:

$$f(\lambda) = b + \sum_k a_k \exp \left[-\frac{(\lambda - \lambda_k^0)^2}{2w_k^2} \right]. \quad (3)$$

Here λ is the rest frame wavelength, a_k , λ_k , w_k are the amplitudes, the central wavelengths and FWHM (up to factor of $\sqrt{2}$) of each k -th emission feature, and b is the constant describing continuum.

Because we are interested more in parameters of the lines rather than the global fit of all Ly α forest region with one function, we split this region onto three parts corresponding to each emission feature (multiplet) and fit each part separately. The fitting procedure was conducted in the following two steps: (i) using the IDL `lmfit` subroutine for each multiplet (with central wavelengths around 1070, 1120 and 1215 Å) the best fit model in a form of (3) was found; (ii) the central wavelengths λ^0 obtained at the first step were fixed and the best fit values of other parameters $\{b, a_k, w_k\}$ with the 1σ errors from the extremal values of the N-dimensional distribution were calculated by the Markov Chain Monte Carlo (MCMC) method using `CosmoMC` package as a generic sampler (with the values of $\{b, a_k, w_k\}$ obtained previously as starting values). The MCMC technique

has been chosen as it is fast and accurate method of exploration of high-dimensional parameter spaces. In each case we generated 8 chains which have converged to $R-1 < 0.0075$.

Due to the small values of amplitudes of these lines comparing with the Ly α emission line, the central wavelength of Ly α was determined separately from the red part of the third multiplet and then fixed. Note that we used only the wavelength range up to 1185 Å for this multiplet, thus we ignored its tiny structure at longer wavelengths and assumed the redward part of 1185 Å to be only one line with the central wavelength about 1215 Å.

Due to the small values the flux dispersion, σ_f^2 , in composite spectra determined from the covariance matrix to estimate errors correctly we introduced additional intrinsic errors, σ_{int} , determined such as the total dispersion, $\sigma^2 = \sigma_f^2 + \sigma_{int}^2$, is such resulting the minimal $\chi^2/\text{d.o.f.}$ to be $1 - 0$.

4 THE RESULTS

4.1 Line identification

The central wavelengths of all the lines found in composite spectra are presented in Table 2. Only the lines for which the parameters were calculated with the help of MCMC method are presented. The arrows stand for regions for which the fit failed, ‘tent.’ means tentative identification by eye (which was not included in fit). Despite of variance in central wavelengths and the number of lines in different spectra we tried to systematize them. In most cases, except the multiplet around 1120 Å, the lines seem to be the same in all spectra, but due to the difference in their FWHM in one spectrum two given lines are resolved, while in another spectrum they are blended and appear to be fitted better with one Gaussian. The values in brackets mean such doublets fitted by one Gaussian in case of triplets.

The line identifications were taken from the papers on composite UV spectra of quasars obtained with HST and FUSE missions (Zheng et al. 1997; Telfer et al. 2002; Scott et al. 2004), high-resolution spectra of single quasars Ton34 (Binette & Krongold 2008) and PHL1811 (Leighly et al. 2007), and also composite spectra of quasars from optical ground Kast (Tytler et al. 2004) and SDSS (Vanden Berk et al. 2001) surveys (see Table 4.3). The lines which were not identified with known lines from these papers are labelled with $X_1 - X_{10}$.

4.2 Parameters of lines and continuum

The obtained values of the line parameters along with their 1σ errors from the extremal values of the N-dimensional distribution are presented in Tables 4-19, the values of constant b for each multiplet are presented in Table 2. The spectra together with the best fits to multiplets and the lines found are presented in Figures 9-10. As one can see from Table 2 in most cases the values of continuum parameter b within each spectrum vary from one multiplet to another within errors and thus the ‘true’ continuum within this wavelength range can be considered as a constant rather than having the same power-law form as that within longer wavelength range.

Table 2. The values of constant b characterizing the ‘true’ continuum for each multiplet. Here n is the number of spectrum.

| n | mult. 1 | mult. 2 | mult. 3 |
|-----|---------------------------|---------------------------|---------------------------|
| 1 | $0.943^{+0.020}_{-0.050}$ | $0.954^{+0.006}_{-0.010}$ | $0.974^{+0.014}_{-0.034}$ |
| 2 | $0.966^{+0.022}_{-0.046}$ | $0.976^{+0.008}_{-0.011}$ | $0.999^{+0.019}_{-0.083}$ |
| 3 | $0.973^{+0.014}_{-0.027}$ | $0.997^{+0.005}_{-0.010}$ | $1.016^{+0.021}_{-0.033}$ |
| 4 | $0.978^{+0.029}_{-0.044}$ | $0.958^{+0.012}_{-0.014}$ | $1.048^{+0.014}_{-0.027}$ |
| 5 | $1.011^{+0.006}_{-0.006}$ | $1.003^{+0.007}_{-0.015}$ | $1.011^{+0.014}_{-0.020}$ |
| 6 | — | $1.000^{+0.006}_{-0.009}$ | $1.074^{+0.017}_{-0.021}$ |
| 7 | $1.044^{+0.013}_{-0.039}$ | $1.048^{+0.015}_{-0.071}$ | $1.085^{+0.022}_{-0.030}$ |
| 8 | $1.078^{+0.043}_{-0.058}$ | $1.009^{+0.026}_{-0.039}$ | $1.099^{+0.010}_{-0.013}$ |
| 9 | $1.067^{+0.006}_{-0.008}$ | $1.008^{+0.020}_{-0.025}$ | $1.101^{+0.025}_{-0.032}$ |
| 10 | $1.073^{+0.017}_{-0.027}$ | $1.089^{+0.009}_{-0.024}$ | $1.089^{+0.014}_{-0.020}$ |
| 11 | $1.066^{+0.010}_{-0.011}$ | $1.077^{+0.011}_{-0.022}$ | $1.125^{+0.016}_{-0.025}$ |
| 12 | $1.106^{+0.033}_{-0.044}$ | $1.128^{+0.009}_{-0.022}$ | $1.171^{+0.024}_{-0.046}$ |
| 13 | $1.142^{+0.007}_{-0.009}$ | $1.121^{+0.006}_{-0.008}$ | $1.120^{+0.009}_{-0.013}$ |
| 14 | — | $1.136^{+0.007}_{-0.012}$ | $1.149^{+0.007}_{-0.009}$ |
| 15 | $1.155^{+0.017}_{-0.089}$ | $1.157^{+0.007}_{-0.013}$ | — |
| 16 | $1.146^{+0.008}_{-0.007}$ | $1.124^{+0.009}_{-0.009}$ | $1.126^{+0.013}_{-0.040}$ |

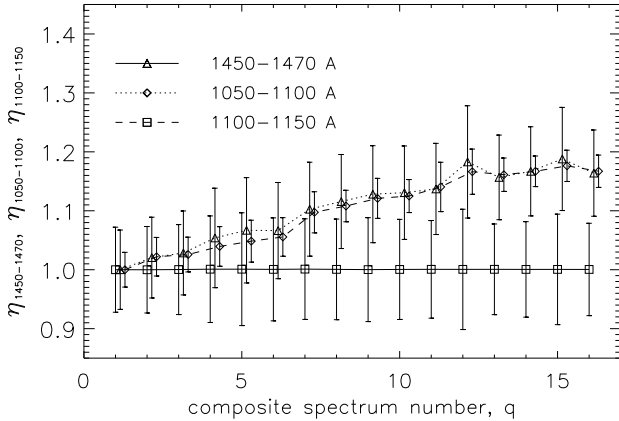


Figure 8. Ratio of the mean flux, η_k , in each composite spectrum and composite spectrum with $\alpha_\lambda = -0.84$, η_0 , within the wavelength range 1450 – 1470, 1050 – 1100 and 1100 – 1150 Å.

4.3 Normalization constant

As one can see from increasing of the b values with increasing of α_λ (Sec. 4.2), the first step of the composite spectrum generation, normalization of individual spectra on the mean flux within 1450 – 1470 Å range, introduces additional uncertainties into the composite spectra when stacking spectra with different slopes α_λ together in one composite. In Figure 8 the dependence of the following value

$$\eta = \frac{\langle f_i \rangle_q}{\langle f_i \rangle_0}$$

on the number q of the composite spectrum is presented for illustration of this fact in Figure 4.2 for wavelength ranges 1450 – 1470, 1050 – 1100 and 1100 – 1150 Å, where the last two ranges are located within the Ly α forest. Here $\langle f_i \rangle$ is the mean flux within the given wavelength range. As one can see from this figure, this deviation of η from unity for spectra with different slopes, which has to cause additional

uncertainty in estimation of the mean transmission value \bar{F} , is about 20 %.

5 DISCUSSION AND CONCLUSIONS

We presented a new approach for composite spectra generation, which lies in stacking only the quasar spectra with similar slope α_λ within the range redward of Ly α emission line (1215.67 Å). The motivation for this is the following. The quasar spectra in UV range have similar general form: bump-shaped continuum (with maximum around 1000 – 1300 Å), the nature of which is still not clear, with broad emission lines similar for all quasars. According to the unification scheme of active galactic nuclei this ultraviolet bump is formed in accretion disc, hence its shape should reflect somehow the physical conditions inside the accretion disc. Independent on given underlying physics itself one can assume that the similarity in shape of one wavelength range of the spectrum can imply the similarity in shape of nearby ranges. Using own sample of quasar spectra from the 7th data release of SDSS we determined the slopes α_λ of continuum within the range 1278 – 1480 Å considering it to be a power-law $\sim \lambda_\alpha$ and generated 16 composites stacking the spectra with similar slopes. This technique allowed us to reduce the noise and revealed more tiny features than in case of composite spectra made stacking spectra with different slopes.

Considering the wavelength range $\lambda \approx 1050 - 1200$ Å known as the Ly α -forest region we found more than 14 lines within it, three of which were found in previous studies of quasar composite spectra from SDSS by Vanden Berk et al. (2001), some others were found in composite spectra from space-based HST and FUSE telescopes (Scott et al. 2004; Telfer et al. 2002; Zheng et al. 1997) or high-resolution spectra of individual quasars from ground-based telescopes (Binette & Krongold 2008; Leighly et al. 2007; Tytler et al. 2004). The parameters of the lines were calculated with the help of MCMC method.

Summing up the results we have to note the following.

- Using the proposed approach helps to reduce the noise in composite spectra and study them more carefully.
- Any dependence of the shape of quasar spectrum within the range $\sim 1050 - 1480$ Å (defined by the slope of continuum within 1278 – 1480 Å) on luminosity in SDSS u , g , r and i bands as far as on luminosity in 1450 – 1470 Å band (which is the closest to the bump region available for study due to absence of emission and absorption lines) was not found.
- It was shown that the ‘true’ continuum level within the Ly α -forest region cannot be considered as a power-law with the same slope as in the region redward of Ly α emission line.

The absence of dependence of the UV-bump shape on luminosity in the bands mentioned above requires the further study of this region (e.g. more careful study of the region redward of Ly α emission line), for understanding the physics behind the difference in the UV-bump shape in spectra of different quasars. It is worth to note that the absolute magnitudes in given bands used as a characteristic of luminosity include K-correction which is determined within the frame of some model of the spectrum general shape.

The proposed approach can be applied for generation

Table 4. Emission lines with their measured rest-frame wavelengths found in individual or composite spectra of quasars within the range between Ly α and Ly β emission lines from previous studies. The brackets in case of ArI and NII mean that in corresponding paper the authors speak about doublet of ArI+NII.

| line λ_{lab} , Å | SIV | ArI 1066.66 | NII 1085.12 | SiIII* 1111.59 | FeIII | CIII* 1175.67 | SiII 1194.12 | SiIII |
|-----------------------------|-----------|----------------|----------------|-------------------|---------|------------------|-----------------|-------|
| Zheng et al. (1997) | | tent. | | | | | | |
| Telfer et al. (2002) | | [1065] | | | 1123 | 1176 | 1195 | |
| Scott et al. (2004) | 1062+1073 | | [1084] | | | | | |
| Binette & Krongold (2008) | 1067 | | [1084] | | 1123 | 1176 | 1194 | 1207 |
| Leighly et al. (2007) | | | 1084.2 | 1110.5 | | 1175.4 | 1193.6 | |
| Tytler et al. (2004) | | [1070.95] | | | 1123.13 | 1175.88 | | |
| Vanden Berk et al. (2001) | | 1065.10 | | | 1117.26 | 1175.35 | | |

of new templates for more precise quasar redshift measurements with the common cross-correlation technique used in redshift surveys, more precise theoretical determination of K-correction and color-indexes, as far as for determination of continuum and mean transmission in Ly α forest studies. It is also worth to note, that this approach reduces the uncertainties in the mean transmission caused by using the composite spectra made with common approach, which can constitute about 20%.

ACKNOWLEDGEMENTS

This work has been supported by Swiss National Science Foundation (SCOPES grant No 128040).

The authors are thankful to the Sloan Digital Sky Survey team. Funding for the SDSS has been provided by the Alfred P. Sloan Foundation, the Participating Institutions, the National Aeronautics and Space Administration, the National Science Foundation, the US Department of Energy, the Japanese Monbukagakusho, and the Max Planck Society. The SDSS Web site is <http://www.sdss.org>.

The authors are thankful to Mariangela Bernardi, Ravi K. Sheth and Ievgen Vovk for fruitful discussions.

The authors also acknowledge the usage of **CosmoMC** package.

REFERENCES

- Abazajian K. N., Adelman-McCarthy J. K., Agüeros M. A., Allam S. S., Allende Prieto C., An D., Anderson K. S. J., Anderson S. F., Annis J., Bahcall N. A., et al. 2009, *ApJS*, 182, 543
- Becker G. D., Rauch M., Sargent W. L. W., 2007, *ApJ*, 662, 72
- Bernardi M., Sheth R. K., SubbaRao M., Richards G. T., Burles S., Connolly A. J., Frieman J., Nichol R., Schaye J., Schneider D. P., Vanden Berk D. E., York D. G., Brinkmann J., Lamb D. Q., 2003, *AJ*, 125, 32
- Binette L., Krongold Y., 2008, *ap*, 477, 413
- Brotherton M. S., Tran H. D., Becker R. H., Gregg M. D., Laurent-Muehleisen S. A., White R. L., 2001, *ApJ*, 546, 775
- Cappetta M., D’Odorico V., Cristiani S., Saitta F., Viel M., 2010, *MNRAS*, 407, 1290
- Carballo R., González-Serrano J. I., Benn C. R., Sánchez S. F., Vigotti M., 1999, *MNRAS*, 306, 137
- Desjacques V., Nusser A., Sheth R. K., 2007, *MNRAS*, 374, 206
- D’Odorico V., Viel M., Saitta F., Cristiani S., Bianchi S., Boyle B., Lopez S., Maza J., Outram P., 2006, *MNRAS*, 372, 1333
- Faucher-Giguère C., Prochaska J. X., Lidz A., Hernquist L., Zaldarriaga M., 2008, *ApJ*, 681, 831
- Francis P. J., Hewett P. C., Foltz C. B., Chaffee F. H., Weymann R. J., Morris S. L., 1991, *ApJ*, 373, 465
- Hewett P. C., Wild V., 2010, *MNRAS*, 405, 2302
- Kim T., Viel M., Haehnelt M. G., Carswell R. F., Cristiani S., 2004, *MNRAS*, 347, 355
- Leighly K. M., Halpern J. P., Jenkins E. B., Casebeer D., 2007, *ApJS*, 173, 1
- McDonald P., Miralda-Escudé J., Rauch M., Sargent W. L. W., Barlow T. A., Cen R., Ostriker J. P., 2000, *ApJ*, 543, 1
- McDonald P., Seljak U., Burles S., Schlegel D. J., Weinberg D. H., Cen R., Shih D., Schaye J., Schneider D. P., Bahcall N. A., 2006, *ApJS*, 163, 80
- Menou K., Vanden Berk D. E., Ž. Ivezić Kim R. S. J., Knapp G. R., Richards G. T., Strateva I., Fan X., Gunn J. E., Hall P. B., 2001, *ApJ*, 561, 645
- Pieri M. M., Frank S., Weinberg D. H., Mathur S., York D. G., 2010, *ApJ*, 724, L69
- Polinovskyi G., Malygin M., 2010, in *WDS’10 Proceedings of Contributed Papers: Part III – Physics*, p.163-168 Mean Transmitted Flux in the Ly α Forest from a Sample of 2QZ Quasars. pp 163–168
- Press W. H., Rybicki G. B., Schneider D. P., 1993, *ApJ*, 414, 64
- Richards G. T., Strauss M. A., Fan X., Hall P. B., Jester S., Schneider D. P., Vanden Berk D. E., Stoughton C., Anderson S. F., Brunner R. J., Gray J., 2006, *AJ*, 131, 2766
- Schlegel D. J., Finkbeiner D. P., Davis M., 1998, *ApJ*, 500, 525
- Schneider D. P., Richards G. T., Hall P. B., Strauss M. A., Anderson S. F., Boroson T. A., Ross N. P., Shen Y., Brandt 2010, *AJ*, 139, 2360
- Scott J., Kriss G., Brotherton M., Green R., Hutchings J., Shull J., Zheng W., 2004, in G. T. Richards & P. B. Hall ed., *AGN Physics with the Sloan Digital Sky Survey Vol. 311 of Astronomical Society of the Pacific Conference Series, A Composite Extreme Ultraviolet QSO Spectrum*

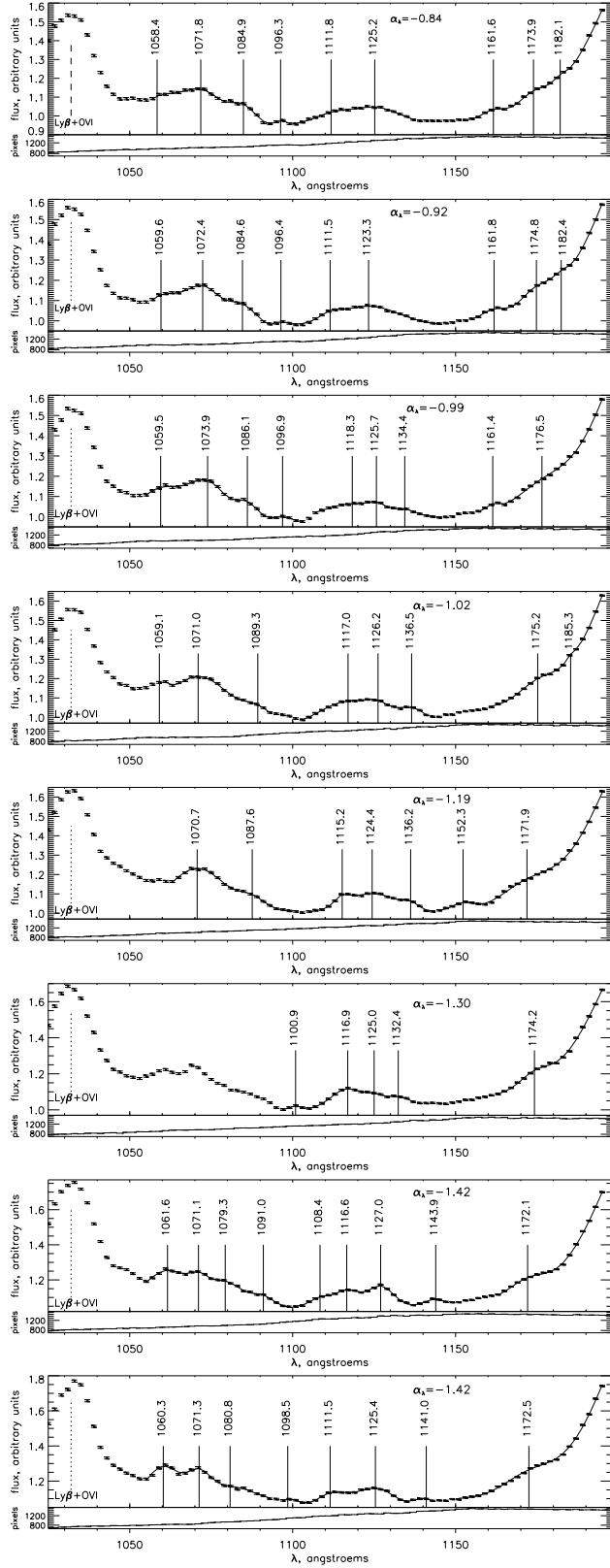


Figure 9. Composite spectra 1–8 with α_λ (from top to bottom): $-0.84, -0.92, -0.99, -1.02, -1.19, -1.30, -1.42, -1.42$.

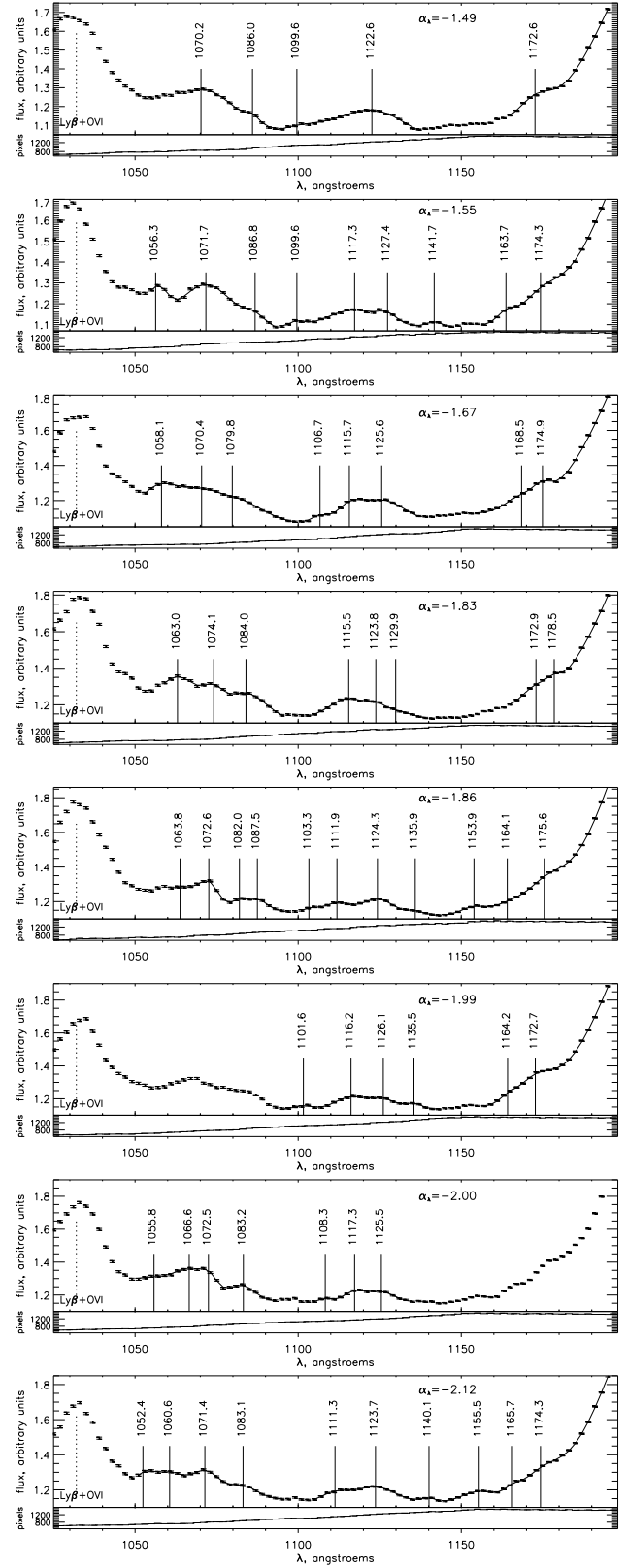


Figure 10. Composite spectra 9–16 with α_λ (from top to bottom): $-1.49, -1.55, -1.67, -1.83, -1.86, -1.99, -2.00, -2.12$.

- from FUSE. pp 31–+
- Songaila A., 2004, *AJ*, 127, 2598
- Telfer R. C., Zheng W., Kriss G. A., Davidsen A. F., 2002, *ApJ* , 565, 773
- Tytler D., O’Meara J. M., Suzuki N., Kirkman D., Lubin D., Orin A., 2004, *AJ*, 128, 1058
- Vanden Berk D. E., Richards G. T., Bauer A., Strauss M. A., Schneider D. P., Heckman T. M., York D. G., Hall P. B., Fan X., Knapp G. R., 2001, *AJ*, 122, 549
- Weymann R. J., Vogel S. N., Veilleux S., Epps H. W., 2001, *ApJ* , 561, 559
- Wild V., Hewett P. C., 2005, *MNRAS* , 358, 1083
- Wild V., Hewett P. C., 2010, *ArXiv e-prints*
- Wolfe A. M., Gawiser E., Prochaska J. X., 2005, *ARA&A*, 43, 861
- Zheng W., Kriss G. A., Telfer R. C., Grimes J. P., Davidsen A. F., 1997, *ApJ* , 475, 469

Table 3. Emission lines found in spectra. Lines in brackets are doublets in case of triplets. Arrows stand for failed fit.

| | 1 | 2 | 3 | 4 | 5 | 6 | 7 | |
|----|----------------|------------------------------------|--------------------|--------------------------------|-----------------------------|----------------|--------------------------------------|------------------------------|
| | X ₁ | X ₂ +ArI+X ₃ | NII+X ₄ | X ₅ +X ₆ | FeIII-multiplet | X ₇ | X ₈ +CIII*+X ₉ | X ₁₀ +Ly α |
| 1 | tent. | 1058.4+[1071.8] | 1084.9 | 1096.3 | 1111.8+1125.2 | | 1161.6+1173.9+1182.1 | 1214.4 |
| 2 | tent. | 1059.6+[1072.4] | 1084.6 | 1096.4 | 1111.5+1123.3 | tent. | 1161.8+1174.8+1182.4 | 1214.3 |
| 3 | tent. | 1059.5+[1073.9] | 1086.1 | 1096.9 | 1118.3+1125.7+1134.4 | tent. | 1161.4+[1176.5] | 1214.2 |
| 4 | tent. | 1059.5+[1071.0] | 1089.3 | tent. | 1117.0+1126.2+1136.5 | tent. | tent.+1175.2+1185.3 | 1214.7 |
| 5 | tent. | tent.+ [1070.7] | 1087.6 | | 1115.2+1124.4+1136.2 | 1152.3 | 1171.9 | 1214.3 |
| 6 | → | → | → | 1100.9 | 1116.9+1125.0+1132.4 | tent. | tent.+[1174.2] | 1213.2 |
| 7 | → | 1061.6+[1071.1] | 1079.3+1091.0 | | 1108.4+1116.6+1127.0+1143.9 | | tent.+[1172.1] | 1213.2 |
| 8 | → | 1060.3+[1071.3] | 1080.8 | 1098.5 | 1111.5+1125.4+1141.0 | tent. | 1172.5 | 1213.8 |
| 9 | → | tent.+[1070.2] | 1086.0 | 1099.6 | 1122.6 | tent. | 1172.6 | 1213.4 |
| 10 | → | 1056.3+[1071.7] | 1086.8 | 1099.6 | 1117.3+1127.4+1141.7 | tent. | 1163.7+[1174.2] | 1213.8 |
| 11 | → | 1058.1+[1070.4] | 1079.9 | | 1106.7+1115.7+ 1125.6 | tent. | [1168.5]+1174.9 | 1213.8 |
| 12 | → | [1063.0]+1074.1 | 1084.0 | | 1115.5+1123.8+1129.0 | | tent.+1172.9+1178.5 | 1214.4 |
| 13 | → | [1063.8]+1072.6 | 1082.0+1087.5 | 1103.3 | 1111.9+1124.3+1135.9 | 1153.9 | 1164.1+[1172.7] | 1214.5 |
| 14 | → | → | → | 1101.6 | 1116.2+1126.2+1135.5 | tent. | 1172.0 | 1214.4 |
| 15 | 1055.8 | [1066.6]+1072.5 | 1083.2 | tent. | 1108.3+1117.3+1125.5+tent. | ← | ← | ← |
| 16 | 1052.4 | 1060.6+[1071.4] | 1083.1 | tent. | 1111.3+1123.7+1140.1 | 1155.5 | 1165.7+[1174.3] | 1214.1 |

Table 5. Parameters of emission lines for spectrum 1 with $\alpha_\lambda = -0.84$.

| $\lambda_0, \text{\AA}$ | 1058.4 | 1071.8 | 1084.9 | 1096.3 | 1111.8 | 1125.2 | 1161.6 | 1173.9 | 1182.1 | 1214.4 |
|-------------------------|---------------------------|---------------------------|---------------------------|---------------------------|---------------------------|---------------------------|---------------------------|---------------------------|---------------------------|---------------------------|
| a | $0.137^{+0.060}_{-0.034}$ | $0.191^{+0.028}_{-0.023}$ | $0.093^{+0.054}_{-0.031}$ | $0.024^{+0.028}_{-0.013}$ | $0.047^{+0.008}_{-0.009}$ | $0.091^{+0.008}_{-0.008}$ | $0.046^{+0.029}_{-0.018}$ | $0.089^{+0.017}_{-0.016}$ | $0.030^{+0.047}_{-0.021}$ | $1.118^{+0.072}_{-0.074}$ |
| w, \AA | $5.6^{+1.5}_{-0.8}$ | $6.7^{+1.4}_{-0.9}$ | $3.8^{+2.0}_{-1.0}$ | $1.3^{+1.4}_{-0.8}$ | $5.3^{+1.3}_{-0.9}$ | $7.7^{+1.3}_{-0.8}$ | $3.2^{+2.9}_{-1.4}$ | $5.2^{+1.5}_{-1.1}$ | $1.9^{+1.8}_{-1.4}$ | $17.2^{+1.0}_{-0.7}$ |

Table 6. Parameters of emission lines for spectrum 2 with $\alpha_\lambda = -0.92$.

| $\lambda_0, \text{\AA}$ | 1059.6 | 1072.4 | 1084.6 | 1096.4 | 1111.5 | 1123.3 | 1161.8 | 1174.8 | 1182.4 | 1214.3 |
|-------------------------|---------------------------|---------------------------|---------------------------|---------------------------|---------------------------|---------------------------|---------------------------|---------------------------|---------------------------|---------------------------|
| a | $0.150^{+0.049}_{-0.028}$ | $0.197^{+0.019}_{-0.018}$ | $0.102^{+0.048}_{-0.026}$ | $0.018^{+0.021}_{-0.012}$ | $0.030^{+0.009}_{-0.007}$ | $0.096^{+0.010}_{-0.008}$ | $0.049^{+0.074}_{-0.019}$ | $0.100^{+0.029}_{-0.016}$ | $0.030^{+0.035}_{-0.014}$ | $1.101^{+0.087}_{-0.057}$ |
| w, \AA | $5.6^{+1.5}_{-0.9}$ | $5.5^{+0.6}_{-0.4}$ | $4.3^{+1.7}_{-1.0}$ | $1.9^{+1.7}_{-1.5}$ | $3.1^{+0.9}_{-0.7}$ | $9.5^{+1.3}_{-1.2}$ | $3.4^{+4.5}_{-1.4}$ | $5.1^{+0.9}_{-1.2}$ | $2.0^{+1.4}_{-1.0}$ | $17.0^{+1.3}_{-0.8}$ |

Table 7. Parameters of emission lines for spectrum 3 with $\alpha_\lambda = -0.99$.

| $\lambda_0, \text{\AA}$ | 1059.5 | 1073.9 | 1086.1 | 1096.9 | 1118.3 | 1125.7 | 1134.4 | 1161.4 | 1176.5 | 1214.2 |
|-------------------------|---------------------------|---------------------------|---------------------------|---------------------------|---------------------------|---------------------------|---------------------------|---------------------------|---------------------------|---------------------------|
| a | $0.165^{+0.029}_{-0.019}$ | $0.190^{+0.032}_{-0.022}$ | $0.084^{+0.021}_{-0.019}$ | $0.029^{+0.025}_{-0.019}$ | $0.067^{+0.011}_{-0.007}$ | $0.031^{+0.006}_{-0.010}$ | $0.032^{+0.006}_{-0.006}$ | $0.029^{+0.025}_{-0.022}$ | $0.101^{+0.033}_{-0.029}$ | $1.147^{+0.109}_{-0.116}$ |
| w, \AA | $6.9^{+1.2}_{-0.8}$ | $5.7^{+0.5}_{-0.4}$ | $3.4^{+0.6}_{-0.6}$ | $2.7^{+3.2}_{-1.6}$ | $8.1^{+1.0}_{-0.7}$ | $2.6^{+0.8}_{-0.7}$ | $3.8^{+2.4}_{-0.8}$ | $2.0^{+3.6}_{-1.2}$ | $7.6^{+2.0}_{-1.6}$ | $16.0^{+0.9}_{-0.7}$ |

Table 8. Parameters of emission lines for spectrum 4 with $\alpha_\lambda = -1.02$.

| $\lambda_0, \text{\AA}$ | 1059.5 | 1071.0 | 1089.3 | 1117.0 | 1126.2 | 1136.5 | 1175.2 | 1185.3 | 1214.7 |
|-------------------------|---------------------------|---------------------------|---------------------------|---------------------------|---------------------------|---------------------------|---------------------------|---------------------------|---------------------------|
| a | $0.096^{+0.035}_{-0.016}$ | $0.234^{+0.045}_{-0.032}$ | $0.051^{+0.039}_{-0.023}$ | $0.124^{+0.015}_{-0.014}$ | $0.055^{+0.007}_{-0.007}$ | $0.084^{+0.010}_{-0.010}$ | $0.091^{+0.025}_{-0.017}$ | $0.025^{+0.055}_{-0.018}$ | $1.227^{+0.157}_{-0.098}$ |
| w, \AA | $2.4^{+0.5}_{-0.4}$ | $9.5^{+1.0}_{-0.8}$ | $3.9^{+2.0}_{-1.4}$ | $8.3^{+0.7}_{-0.7}$ | $3.5^{+0.5}_{-0.4}$ | $4.7^{+0.6}_{-0.5}$ | $5.9^{+2.2}_{-1.2}$ | $1.4^{+2.7}_{-1.2}$ | $16.1^{+0.7}_{-1.2}$ |

Table 9. Parameters of emission lines for spectrum 5 with $\alpha_\lambda = -1.19$.

| $\lambda_0, \text{\AA}$ | 1070.7 | 1087.6 | 1115.2 | 1124.4 | 1136.2 | 1152.3 | 1171.9 | 1214.3 |
|-------------------------|---------------------------|---------------------------|---------------------------|---------------------------|---------------------------|---------------------------|---------------------------|---------------------------|
| a | $0.221^{+0.009}_{-0.008}$ | $0.055^{+0.010}_{-0.011}$ | $0.043^{+0.010}_{-0.010}$ | $0.100^{+0.014}_{-0.007}$ | $0.029^{+0.009}_{-0.011}$ | $0.038^{+0.019}_{-0.015}$ | $0.108^{+0.020}_{-0.017}$ | $1.122^{+0.065}_{-0.063}$ |
| w, \AA | $8.6^{+0.5}_{-0.5}$ | $3.8^{+0.9}_{-0.7}$ | $2.2^{+0.5}_{-0.5}$ | $8.0^{+1.9}_{-1.2}$ | $2.2^{+0.7}_{-0.7}$ | $3.2^{+1.6}_{-1.3}$ | $7.9^{+1.1}_{-1.0}$ | $17.5^{+0.5}_{-0.5}$ |

Table 10. Parameters of emission lines for spectrum 6 with $\alpha_\lambda = -1.30$.

| $\lambda_0, \text{\AA}$ | 1100.9 | 1116.9 | 1125.0 | 1132.4 | 1174.2 | 1213.2 |
|-------------------------|---------------------------|---------------------------|---------------------------|---------------------------|---------------------------|---------------------------|
| a | $0.024^{+0.007}_{-0.009}$ | $0.118^{+0.008}_{-0.006}$ | $0.040^{+0.010}_{-0.010}$ | $0.073^{+0.009}_{-0.006}$ | $0.075^{+0.020}_{-0.017}$ | $1.119^{+0.080}_{-0.070}$ |
| w, \AA | $1.5^{+0.9}_{-0.4}$ | $5.1^{+0.4}_{-0.3}$ | $2.6^{+0.4}_{-0.4}$ | $4.7^{+0.7}_{-0.6}$ | $4.6^{+1.6}_{-1.1}$ | $17.1^{+0.6}_{-0.6}$ |

Table 11. Parameters of emission lines for spectrum 7 with $\alpha_\lambda = -1.42$.

| $\lambda_0, \text{\AA}$ | 1061.6 | 1071.1 | 1079.3 | 1091.0 | 1108.4 | 1116.6 | 1127.0 | 1143.9 | 1172.1 | 1213.2 |
|-------------------------|---------------------------|---------------------------|---------------------------|---------------------------|---------------------------|---------------------------|---------------------------|---------------------------|---------------------------|---------------------------|
| a | $0.210^{+0.038}_{-0.019}$ | $0.060^{+0.027}_{-0.034}$ | $0.137^{+0.022}_{-0.019}$ | $0.052^{+0.041}_{-0.025}$ | $0.050^{+0.060}_{-0.031}$ | $0.093^{+0.024}_{-0.018}$ | $0.117^{+0.065}_{-0.023}$ | $0.042^{+0.067}_{-0.020}$ | $0.084^{+0.025}_{-0.019}$ | $1.158^{+0.075}_{-0.053}$ |
| w, \AA | $7.4^{+1.5}_{-0.9}$ | $2.4^{+0.8}_{-0.9}$ | $5.9^{+1.6}_{-1.0}$ | $3.1^{+2.5}_{-1.3}$ | $2.8^{+5.2}_{-1.2}$ | $3.8^{+1.4}_{-0.8}$ | $3.8^{+1.9}_{-0.8}$ | $3.3^{+3.7}_{-1.9}$ | $5.4^{+1.5}_{-1.1}$ | $16.2^{+0.4}_{-0.4}$ |

Table 12. Parameters of emission lines for spectrum 8 with $\alpha_\lambda = -1.42$.

| $\lambda_0, \text{\AA}$ | 1060.3 | 1071.3 | 1080.8 | 1098.5 | 1111.5 | 1125.4 | 1141.0 | 1172.5 | 1213.8 |
|-------------------------|---------------------------|---------------------------|---------------------------|---------------------------|---------------------------|---------------------------|---------------------------|---------------------------|---------------------------|
| a | $0.203^{+0.046}_{-0.046}$ | $0.132^{+0.027}_{-0.045}$ | $0.088^{+0.064}_{-0.049}$ | $0.085^{+0.035}_{-0.025}$ | $0.107^{+0.036}_{-0.022}$ | $0.149^{+0.040}_{-0.027}$ | $0.082^{+0.036}_{-0.022}$ | $0.112^{+0.015}_{-0.014}$ | $1.251^{+0.065}_{-0.068}$ |
| w, \AA | $5.2^{+1.8}_{-1.0}$ | $3.4^{+0.8}_{-0.9}$ | $7.7^{+3.1}_{-3.8}$ | $3.8^{+1.2}_{-0.9}$ | $5.0^{+0.6}_{-0.5}$ | $6.6^{+0.8}_{-0.6}$ | $3.8^{+1.3}_{-0.7}$ | $7.7^{+1.3}_{-1.1}$ | $16.4^{+0.5}_{-0.4}$ |

Table 13. Parameters of emission lines for spectrum 9 with $\alpha_\lambda = -1.49$.

| $\lambda_0, \text{\AA}$ | 1070.2 | 1086.0 | 1099.6 | 1122.6 | 1172.6 | 1213.4 |
|-------------------------|---------------------------|---------------------------|---------------------------|---------------------------|---------------------------|---------------------------|
| a | $0.225^{+0.007}_{-0.006}$ | $0.034^{+0.008}_{-0.008}$ | $0.077^{+0.018}_{-0.016}$ | $0.169^{+0.026}_{-0.023}$ | $0.094^{+0.025}_{-0.019}$ | $1.079^{+0.065}_{-0.051}$ |
| w, \AA | $9.9^{+0.6}_{-0.5}$ | $1.9^{+0.5}_{-0.5}$ | $9.3^{+2.1}_{-1.2}$ | $10.4^{+0.9}_{-0.8}$ | $4.8^{+1.2}_{-0.9}$ | $17.5^{+0.5}_{-0.5}$ |

Table 14. Parameters of emission lines for spectrum 10 with $\alpha_\lambda = -1.55$.

| $\lambda_0, \text{\AA}$ | 1056.3 | 1071.7 | 1086.8 | 1099.6 | 1117.3 | 1127.4 | 1141.7 | 1163.7 | 1174.3 | 1213.8 |
|-------------------------|---------------------------|---------------------------|---------------------------|---------------------------|---------------------------|---------------------------|---------------------------|---------------------------|---------------------------|---------------------------|
| a | $0.179^{+0.030}_{-0.020}$ | $0.221^{+0.029}_{-0.019}$ | $0.054^{+0.028}_{-0.019}$ | $0.025^{+0.015}_{-0.014}$ | $0.081^{+0.025}_{-0.009}$ | $0.035^{+0.012}_{-0.011}$ | $0.024^{+0.018}_{-0.013}$ | $0.046^{+0.016}_{-0.019}$ | $0.091^{+0.012}_{-0.013}$ | $1.112^{+0.061}_{-0.046}$ |
| w, \AA | $3.3^{+0.5}_{-0.4}$ | $8.1^{+0.9}_{-0.7}$ | $3.3^{+1.5}_{-1.1}$ | $2.1^{+2.3}_{-1.5}$ | $8.0^{+1.8}_{-1.2}$ | $3.0^{+1.1}_{-1.0}$ | $2.2^{+3.8}_{-1.3}$ | $2.8^{+1.2}_{-1.1}$ | $5.7^{+1.6}_{-0.9}$ | $17.9^{+0.8}_{-0.8}$ |

Table 15. Parameters of emission lines for spectrum 11 with $\alpha_\lambda = -1.67$.

| $\lambda_0, \text{\AA}$ | 1058.1 | 1070.4 | 1079.9 | 1106.7 | 1115.7 | 1125.6 | 1168.5 | 1174.9 | 1213.8 |
|-------------------------|---------------------------|---------------------------|---------------------------|---------------------------|---------------------------|---------------------------|---------------------------|---------------------------|---------------------------|
| a | $0.223^{+0.010}_{-0.010}$ | $0.073^{+0.016}_{-0.020}$ | $0.144^{+0.013}_{-0.012}$ | $0.034^{+0.019}_{-0.014}$ | $0.076^{+0.012}_{-0.010}$ | $0.126^{+0.023}_{-0.013}$ | $0.069^{+0.020}_{-0.018}$ | $0.067^{+0.022}_{-0.026}$ | $1.211^{+0.065}_{-0.065}$ |
| w, \AA | $7.3^{+0.9}_{-0.6}$ | $4.7^{+0.7}_{-0.6}$ | $8.6^{+0.7}_{-0.7}$ | $2.4^{+1.7}_{-0.9}$ | $3.6^{+0.7}_{-0.6}$ | $6.9^{+1.0}_{-0.8}$ | $4.6^{+2.5}_{-1.6}$ | $2.6^{+1.0}_{-0.7}$ | $17.3^{+0.7}_{-0.6}$ |

Table 16. Parameters of emission lines for spectrum 12 with $\alpha_\lambda = -1.83$.

| $\lambda_0, \text{\AA}$ | 1063.0 | 1074.1 | 1084.0 | 1115.5 | 1123.8 | 1129.0 | 1172.9 | 1178.5 | 1214.4 |
|-------------------------|---------------------------|---------------------------|---------------------------|---------------------------|---------------------------|---------------------------|---------------------------|---------------------------|---------------------------|
| a | $0.247^{+0.041}_{-0.032}$ | $0.084^{+0.037}_{-0.034}$ | $0.156^{+0.041}_{-0.030}$ | $0.106^{+0.016}_{-0.011}$ | $0.040^{+0.017}_{-0.026}$ | $0.036^{+0.014}_{-0.010}$ | $0.076^{+0.031}_{-0.016}$ | $0.035^{+0.021}_{-0.021}$ | $1.177^{+0.064}_{-0.044}$ |
| w, \AA | $7.3^{+1.3}_{-1.4}$ | $2.8^{+0.7}_{-0.8}$ | $6.4^{+1.6}_{-1.3}$ | $5.8^{+1.5}_{-0.8}$ | $2.5^{+1.1}_{-0.9}$ | $4.0^{+3.1}_{-1.4}$ | $4.0^{+2.1}_{-1.2}$ | $2.0^{+1.1}_{-1.2}$ | $17.3^{+0.7}_{-0.6}$ |

Table 17. Parameters of emission lines for spectrum 13 with $\alpha_\lambda = -1.86$.

| $\lambda_0, \text{\AA}$ | 1063.8 | 1072.6 | 1082.0 | 1087.5 | 1103.3 | 1111.9 | 1124.3 | 1135.9 | 1153.9 | 1164.1 | 1172.7 | 1214.5 |
|-------------------------|---------------------------|---------------------------|---------------------------|---------------------------|---------------------------|---------------------------|---------------------------|---------------------------|---------------------------|---------------------------|---------------------------|---------------------------|
| a | $0.143^{+0.011}_{-0.009}$ | $0.091^{+0.021}_{-0.013}$ | $0.044^{+0.014}_{-0.014}$ | $0.069^{+0.007}_{-0.010}$ | $0.037^{+0.009}_{-0.008}$ | $0.070^{+0.010}_{-0.007}$ | $0.095^{+0.009}_{-0.007}$ | $0.023^{+0.009}_{-0.007}$ | $0.048^{+0.013}_{-0.011}$ | $0.048^{+0.008}_{-0.011}$ | $0.124^{+0.017}_{-0.012}$ | $1.463^{+0.069}_{-0.048}$ |
| w, \AA | $8.8^{+1.3}_{-1.8}$ | $2.7^{+0.4}_{-0.4}$ | $2.0^{+1.0}_{-0.6}$ | $3.0^{+0.8}_{-0.6}$ | $2.7^{+0.9}_{-0.6}$ | $4.1^{+0.5}_{-0.5}$ | $4.8^{+0.4}_{-0.4}$ | $2.7^{+1.3}_{-0.9}$ | $3.8^{+1.3}_{-0.9}$ | $4.3^{+1.1}_{-0.7}$ | $5.8^{+0.9}_{-0.6}$ | $16.9^{+0.3}_{-0.4}$ |

Table 18. Parameters of emission lines for spectrum 14 with $\alpha_\lambda = -1.99$.

| $\lambda_0, \text{\AA}$ | 1101.6 | 1116.2 | 1126.2 | 1135.5 | 1164.2 | 1172.0 | 1214.4 |
|-------------------------|---------------------------|---------------------------|---------------------------|---------------------------|---------------------------|---------------------------|---------------------------|
| a | $0.020^{+0.013}_{-0.010}$ | $0.076^{+0.014}_{-0.014}$ | $0.061^{+0.012}_{-0.013}$ | $0.033^{+0.013}_{-0.013}$ | $0.032^{+0.011}_{-0.013}$ | $0.125^{+0.008}_{-0.008}$ | $1.363^{+0.047}_{-0.043}$ |
| w, \AA | $2.6^{+3.1}_{-1.3}$ | $4.5^{+0.8}_{-0.6}$ | $4.0^{+1.3}_{-0.7}$ | $2.4^{+1.3}_{-1.0}$ | $2.4^{+1.0}_{-0.7}$ | $5.3^{+0.8}_{-0.5}$ | $17.4^{+0.4}_{-0.3}$ |

Table 19. Parameters of emission lines for spectrum 15 with $\alpha_\lambda = -2.00$.

| $\lambda_0, \text{\AA}$ | 1055.8 | 1066.6 | 1072.5 | 1083.2 | 1108.3 | 1117.3 | 1125.5 |
|-------------------------|---------------------------|---------------------------|---------------------------|---------------------------|---------------------------|---------------------------|---------------------------|
| a | $0.155^{+0.085}_{-0.021}$ | $0.080^{+0.024}_{-0.017}$ | $0.083^{+0.038}_{-0.034}$ | $0.072^{+0.033}_{-0.034}$ | $0.023^{+0.012}_{-0.011}$ | $0.064^{+0.009}_{-0.009}$ | $0.062^{+0.013}_{-0.009}$ |
| w, \AA | $15.4^{+13.3}_{-5.5}$ | $3.7^{+1.3}_{-0.8}$ | $2.4^{+1.1}_{-0.7}$ | $3.5^{+1.8}_{-1.5}$ | $1.7^{+1.8}_{-0.9}$ | $3.3^{+0.7}_{-0.5}$ | $3.9^{+1.1}_{-0.7}$ |

Table 20. Parameters of emission lines for spectrum 16 with $\alpha_\lambda = -2.12$.

| $\lambda_0, \text{\AA}$ | 1052.4 | 1060.6 | 1071.4 | 1083.1 | 1111.3 | 1123.7 | 1140.1 | 1155.5 | 1165.7 | 1174.3 | 1214.1 |
|-------------------------|---------------------------|---------------------------|---------------------------|---------------------------|---------------------------|---------------------------|---------------------------|---------------------------|---------------------------|---------------------------|---------------------------|
| a | $0.136^{+0.010}_{-0.010}$ | $0.138^{+0.014}_{-0.016}$ | $0.158^{+0.008}_{-0.008}$ | $0.074^{+0.009}_{-0.009}$ | $0.057^{+0.009}_{-0.008}$ | $0.093^{+0.009}_{-0.009}$ | $0.028^{+0.009}_{-0.010}$ | $0.061^{+0.035}_{-0.012}$ | $0.037^{+0.012}_{-0.016}$ | $0.112^{+0.019}_{-0.012}$ | $1.346^{+0.062}_{-0.053}$ |
| w, \AA | $3.6^{+0.5}_{-0.4}$ | $4.2^{+0.3}_{-0.4}$ | $4.5^{+0.3}_{-0.3}$ | $4.3^{+0.7}_{-0.6}$ | $4.4^{+0.6}_{-0.6}$ | $6.1^{+0.6}_{-0.5}$ | $2.7^{+1.5}_{-1.0}$ | $5.4^{+3.0}_{-1.2}$ | $2.2^{+0.8}_{-0.7}$ | $6.0^{+1.1}_{-0.8}$ | $17.1^{+0.7}_{-0.6}$ |